Mathematics

AIMS Mathematics, 9(5): 12700–12725.
DOI: 10.3934/math.2024621
Received: 19 January 2024
Revised: 28 February 2024
Accepted: 11 March 2024
Published: 02 April 2024

http://www.aimspress.com/journal/Math

Research article

Sensitivity analysis on optimizing heat transfer rate in hybrid nanofluid flow over a permeable surface for the power law heat flux model: Response surface methodology with ANOVA test

S. R. Mishra[1], Subhajit Panda[2], Mansoor Alshehri[3], Nehad Ali Shah[4,*] and Jae Dong Chung[4]

[1] Department of Mathematics, Siksha 'O' Anusandhan Deemed to be University, Bhubaneswar, Odisha 751030, India; Email: satyaranjan_mshr@yahoo.co.in
[2] Centre for Data Science, Siksha 'O' Anusandhan Deemed to be University, Bhubaneswar, Odisha 751030, India; Email: spanda.math@gmail.com
[3] Department of Mathematics, College of Sciences, King Saud University, P.O. Box 2455 Riyadh 11451, Saudi Arabia; Email: mhalshehri@ksu.edu.sa
[4] Department of Mechanical Engineering, Sejong University, Seoul 05006, South Korea; Email: jdchung@sejong.ac.kr

*** Correspondence:** Email: nehadali199@sejong.ac.kr.

Abstract: Joule dissipation has an important role in the conversion of mechanical energy to heat within a fluid due to the internal friction and viscosity. Moreover, Darcy friction is a measure of the resistance to flow in a porous medium. In response to the efficient heat transfer performance, a robust statistical approach was established to optimize the heat transfer rate in a two-dimensional flow of a nanofluid over a permeable surface embedded with a porous matrix. The electrically conducive fluid affected the flow phenomena to include a carbon nanotube nanoparticle in the conventional liquid water for the enhanced heat transfer properties; additionally, the power-law heat flux model was considered. Appropriate transformation rules were adopted to obtain a non-dimensional system that brought a developed model equipped with several factors. The traditional numerical technique (i.e., shooting based Runge-Kutta) was proposed to handle the coupled nonlinear system. Furthermore, the statistical response surface methodology (RSM) was adopted to obtain an efficient optimized model for the heat transportation rate of the considered factors. An analysis of variance (ANOVA) was utilized to validate the result of the regression analysis. However, it was evident that the nanoparticle concentrations were useful to augment the fluid velocity and the temperature distributions; the statistical approach adopted for the heat transfer

rate displayed an optimized effect as compared to a conventional effect.

Keywords: nanofluid; carbon nanotubes; dissipative heat; response surface methodology; analysis of variance
Mathematics Subject Classification: 76-10, 76R10

Nomenclature

M	Magnetic parameter
Da	Porous parameter
Ec	Eckert number
Q	heat source/sink parameter
Re_x	local Reynolds number
C_f	skin friction coefficient
T_0	constant heat flux
B	Magnetic field strength
C_p	Specific heat capacity
ρ	Density
σ	Electrical conductivity
Nu_x	Nusselt number
S	Suction/Injection parameter
v_w	mass flux velocity
q_w	heat flux
SWCNT	Single walled carbon nanotube
MWCNT	Multi walled carbon nanotube
k	Thermal conductivity
Subscript	
f	fluid
nf	nanofluid
hnf	hybrid nanofluid

1. Introduction

Carbon nanotube (CNTs) water-based nanofluids, which are an encouraging development in the field of nanotechnology, blend the remarkable properties of carbon nanotubes with the versatility of water-based fluids. These nanofluids reveal an enhanced thermal conductivity, mechanical strength, and stability, thus making them precious for various applications. Their potential is vast, from heat transfer enhancement in cooling systems to efficient drug delivery in various biomedical fields. The unique combination of carbon nanotubes and water shows innovations in electronics, aerospace, energy systems, and environmental remediation. Joining these skills, carbon nanotube water-based nanofluids solidify the way for groundbreaking solutions across industries. Hossain et al. [1] deliberated on how CNTs affected the magnetized transient mixed convection nanoliquid transportation. This proposed study aimed to reveal how nanofluid's convective thermal transmission

features under the attendance of a magnetized field. The simultaneous interaction of radiation as well as the magnetic effect on nanoliquids comprised of CNTs dissolved in water were explored by Mahabaleshwar et al. [2]. Their investigation centered on the interaction that took place when these nanoliquids were exposed to an extended sheet. Lund et al. [3] conducted a study to explore the mutual effects of radiation and slippage on a nanoliquid comprised of magnetized carbon CNTs dispersed in a hybrid base liquid. An in-depth investigation was carried out by Noranuar et al. [4] to explore the non-coaxial rotating motion features of CNTs comprised of a magnetized Casson nanoliquid that was passed towards a permeable transferrable disc. The dynamics of transient magnetism motion, with CNTs floating in a nanofluid, were studied by Ramzan et al. [5]. Researchers in the field of fundamental research [6–9] have carefully explored the special appearances of CNT nanofluids, such as their stability, viscosity, and thermal conductivity.

The improved thermal conductivity facilitated by nanoparticles is responsible for the dissipation impact in nanocomposites. The augmented heat conductivity is essential to facilitate the quick and efficient release of heat, which augments the overall efficiency of heat exchange systems. This affects applications where effective boiling heat transmission is essential, such as power generation and refrigeration. To better understand the complex process of dissipation in non-Newtonian nanofluids, Amer et al. [10] showed a thorough analysis. This work centered on the dissipation behavior of a nanoliquid within a Darcy porous medium during its influence with a horizontal expanding interface. Using a chemically reactive nanoliquid moving down an expanded sheet while being affected by a magnetized field, Ullah et al. [11] undertook a thorough investigation to determine the significance of thermal density and viscous dissipation in the context of thermal and mass transmissions. With an emphasis on the influence of viscous dissipation, Mahesh et al. [12] explored in detail how radiation impacted the magnetized pair stress hybrid nanoliquid motion towards a porous interface. The radiative interaction with dissipative heat on the thermally buoyant motion properties of a Williamson nanofluid in a parallel channel were thoroughly studied by Pattanaik et al. [13]. After conducting a thorough investigation, Pattnaik et al. [14] were able to compare the free convection phenomenon in polar nanoliquids. The goal of the study was to clarify the complex interactions that occured among dissipative thermal energy and buoyancy-induced forces. In CNT water-based nanofluids, the relationship between Joule dissipation and Darcy friction exhibited a crucial role in understanding their behavior and optimizing their applications. Joule dissipation refers to the adaptation of electrical energy and their transformation into heat when a current passes through a conductive medium such as carbon nanotubes. This occurrence contributes to the thermal conductivity enhancement perceived in various nanofluids. However, Darcy friction relays to the resistance encountered by the fluid as it flows through a porous medium (i.e., the channels formed by aligned carbon nanotubes). The presence of carbon nanotubes modifies the flow characteristics of the nanofluid, thus influencing its viscosity and frictional losses.

In thermal transportation, response surface methodology (RSM) is a crucial and significant tool that delivers an organized and effective way of working that has a noteworthy impact on heat transmission mechanisms. Baithalu et al. [15] carried out an investigation to optimize the shear and coupling drag in the attendance of a magnetized polar dissipative nanoliquid motion through an elongating interface. To optimize the thermal transportation, their work implemented a technique that integrated RSM and an analysis of variance (ANOVA). Panda et al. [16] performed a study to maximize the thermal transmission rate in a three-dimensional (3D) hybridized nanoliquid flow towards a permeable expanding interface, by means of both an RSM and a sensitivity analysis. This study took the interaction of various features into account to improve the efficiency of heat transmission processes. The simultaneous combination of an RSM and a sensitivity analysis has been

implemented in many heat transmission studies [17–19] to optimize heat transportation processes. The RSM was implemented to nanoliquid flow towards a spinning disc in study carried out by Mehmood et al. [20]. Using a stretching sheet in a porous media, Swain et al. [21] examined the effects of viscous dissipation and Joule heating on a magnetohydrodynamic (MHD) flow and heat transmission. Rana [22] studied nonlinear thermal radiation effects and an optimised heat transfer while examining the rheological characteristics of a Buongiorno nanofluid in an inclined annulus heated by convection heating. Several researchers [23–26] have invested their time and knowledge into performing statistical analyses in the field of heat transport. Raza et al. [27] looked at a fractional model that described how a Casson nanofluid with water and kerosene oil would react to an inclining magnetic field. Chu et al. [28] looked into using the Buongiorno's nanofluid model to examine the flow caused by stretching discs when gyrotactic microbes were present. Many researchers [29–32] have focused their attention on examining various aspects of heat transfer events that took place in nanofluids. Furthermore, Rasool et al. [35−38] briefly presented the behaviour of several nanoparticles in various geometries by considering the impact of the magnetic field, thermal radiation, dissipative heat, etc. In their study, they employed various numerical techniques to understand the physical significance of the contributing factors that affected the flow phenomena.

1.1. Primary objective with novelty of the proposed work

The present analysis is devoted to conducting a comprehensive sensitivity evaluation of the optimizing heat transportation rate of a hybridized nanofluid over a permeable surface. The primary focus goes to the application of the power law heat flux model. Specifically, the study explores the effects of various parameters utilizing single walled carbon nanotube (SWCNT) and multi-walled carbon nanotube (MWCNT) nanoparticles in the water as a nanofluid. However, the key factors are as follows:

- Conduct a sensitivity analysis to identify critical constraints that affect heat transfer in the hybrid nanofluid, such as the particle concentration of the nanoparticles and the magnetized parameter.
- Employ the RSM to optimize the heat transportation rate by determining the optimal combination of the parameters involved in designing the model.
- Apply the power law heat flux model to capture the nonlinear behavior of thermal transportation in the hybridized nanofluid system.
- Validate the results and model predictions using the ANOVA test to assess the significance of the selected factors and their interactions, thus providing the optimization strategy.

Furthermore, SWCNTs and MWCNTs exhibit excellent electrical conductivity, which is crucial for applications in electronics, sensors, and conductive films. Additionally, carbon nanotubes demonstrate superior thermal conductivity, making them valuable for thermal management applications. Both nanoparticles possess exceptional mechanical properties, such as high tensile strengths and stiffness.

2. Mathematical modelling

An MHD and the power law heat flux past a permeable surface with a viscous dissipation, Joule heating, and source heating effects were considered in this study. Figure 1 illustrates the physical model and the coordinate system of the current problem with stretching and shrinking conditions.

- The sheet velocity is $u_w(x)\lambda = \alpha x\lambda$, where α is constant and $\lambda < 0$ is for the shrinking sheet.

- Furthermore, v_w is the mass flux velocity, where $v_w < 0$ represents the suction and a uniform magnetized field of strength B is normally applied.
- In addition to this, the sheet surface is governed to a heat flux that varies according to a power law $q_w = T_0 x^2 / \ell^2$, where ℓ is the length and T_0 is the constant heat flux.

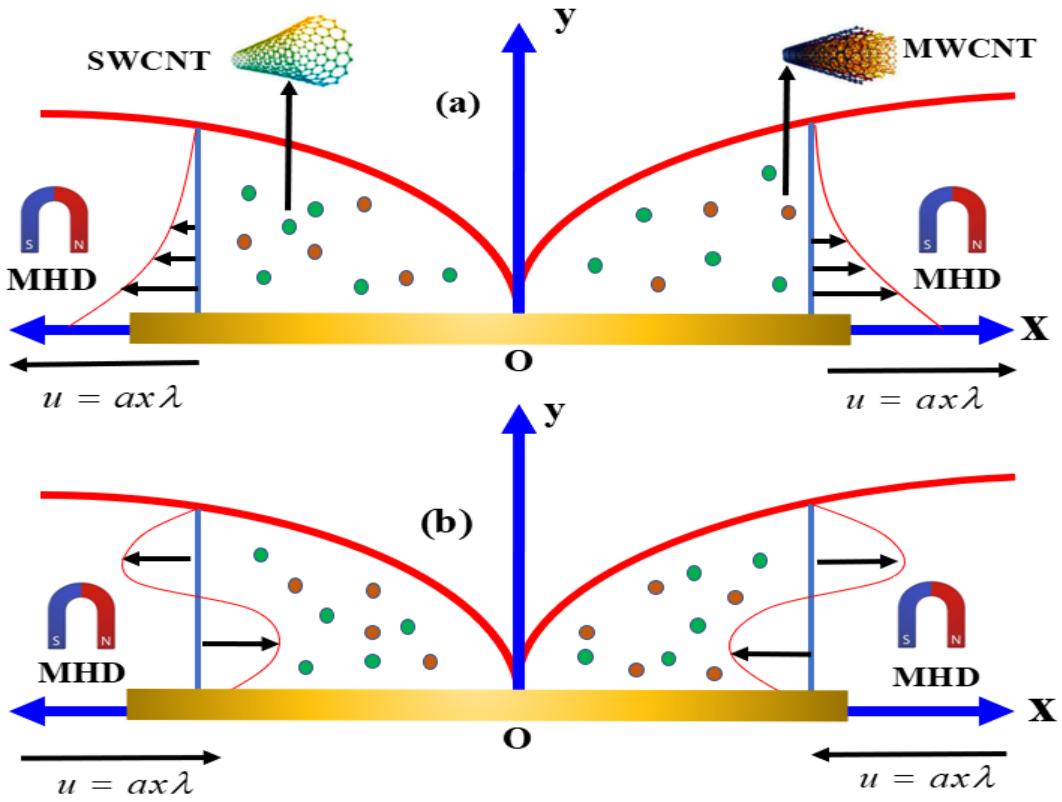

Figure 1. Flow model (a) stretching sheet (b) shrinking sheet.

Given such presumptions, the governing equations can be expressed in the following manner [21]:

$$\partial_x u + \partial_y v = 0, \tag{1}$$

$$u\partial_x u + v\partial_y u = \frac{\mu_{hnf}}{\rho_{hnf}}\partial_{yy} u - \frac{\sigma_{hnf}}{\rho_{hnf}} B^2 u - \frac{\mu_{hnf}}{\rho_{hnf} K^*} u, \tag{2}$$

$$u\partial_x T + v\partial_y T = \frac{k_{hnf}}{\left(\rho C_p\right)_{hnf}}\partial_{yy} T + \frac{Q_0}{\left(\rho C_p\right)_{hnf}}\left(T - T_\infty\right) + \frac{\mu_{hnf}}{\left(\rho C_p\right)_{hnf}}\left(\partial_y u\right)^2 + \frac{\sigma_{hnf}}{\left(\rho C_p\right)_{hnf}} B^2 u^2 + \frac{\mu_{hnf}}{\left(\rho C_p\right)_{hnf} K^*} u^2 \tag{3}$$

subject to

$$\begin{aligned} &u = u_w\left(x\right)\lambda,\ v = v_w,\ -k_{hnf}\partial_y T = q_w \quad \text{at} \quad y = 0, \\ &u \to 0,\ T \to T_\infty, \quad \text{as} \quad y \to \infty. \end{aligned} \tag{4}$$

Here, T and T_∞ represent the hybrid nanofluid temperature and the free stream temperature, respectively, while Q represents the heat source/sink variable. The fluid is a water-based fluid H_2O containing SWCNT and copper MWCNT nanoparticles. The SWCNT ($\phi_1 = \phi_{SWCNT}$) and MWCNT ($\phi_2 = \phi_{MWCNT}$) properties are displayed in Table 1.

Table 1. Thermophysical characteristics [6].

Nanoparticles and Base fluid	$k\ (W/mK)$	$C_p\ (J/kg\,K)$	$\rho\ (kg/m^3)$	σ (s/m)
SWCNT	6600	425	2600	10^6
MWCNT	3000	796	1600	10^7
Water	0.613	4179	997.1	0.005

The thermophysical hybrid nanofluid attributes are stated as follows [6]:

Effective density: $\rho_{\text{hnf}} = (1-\phi_{\text{MWCNT}})\left[(1-\phi_{\text{SWCNT}})\rho_{H_2O} + \phi_{\text{SWCNT}}\rho_{\text{SWCNT}}\right] + \phi_{\text{MWCNT}}\rho_{\text{MWCNT}}$

Dynamic viscosity: $\mu_{\text{hnf}} = \mu_{\text{SWCNT}-H_2O}(0.904)^2 e^{14.8(\phi_{\text{SWCNT}}+\phi_{\text{MWCNT}})}$

Specific heat capacity: $(\rho c_p)_{\text{hnf}} = (1-\phi_{\text{MWCNT}})\left[(1-\phi_{\text{SWCNT}})(\rho c_p)_{H_2O} + \phi_{\text{SWCNT}}(\rho c_p)_{\text{SWCNT}}\right] + \phi_{\text{MWCNT}}(\rho c_p)_{\text{MWCNT}}$

Electrical conductivity: $\dfrac{\sigma_{\text{hnf}}}{\sigma_{\text{SWCNT}-H_2O}} = \dfrac{\sigma_{\text{MWCNT}}(1+2\phi_{\text{MWCNT}}) + 2\sigma_{\text{SWCNT}-H_2O}(1-\phi_{\text{MWCNT}})}{\sigma_{\text{MWCNT}}(1-\phi_{\text{MWCNT}}) + \sigma_{\text{SWCNT}-H_2O}(2+\phi_{\text{MWCNT}})}$,

where $\dfrac{\sigma_{\text{SWCNT}-H_2O}}{\sigma_{H_2O}} = \dfrac{\sigma_{\text{SWCNT}}(1+2\phi_{\text{SWCNT}}) + 2\sigma_{H_2O}(1-\phi_{\text{SWCNT}})}{\sigma_{\text{SWCNT}}(1-\phi_{\text{SWCNT}}) + \sigma_{H_2O}(2+\phi_{\text{SWCNT}})}$.

Thermal conductivity (Hamilton-Crosser model):

$$\frac{k_{\text{hnf}}}{k_{\text{SWCNT}-H_2O}} = \left[\frac{k_{\text{MWCNT}} + (n-1)k_{\text{SWCNT}-H_2O} - (n-1)\phi_{\text{MWCNT}}(k_{\text{SWCNT}-H_2O} - k_{\text{MWCNT}})}{k_{\text{MWCNT}} + (n-1)k_{\text{SWCNT}-H_2O} - \phi_{\text{MWCNT}}(k_{\text{SWCNT}-H_2O} - k_{\text{MWCNT}})}\right],$$

where $\dfrac{k_{\text{SWCNT}-H_2O}}{k_{H_2O}} = \left[\dfrac{k_{\text{SWCNT}} + (n-1)k_{H_2O} - (n-1)\phi_{\text{SWCNT}}(k_{H_2O} - k_{\text{SWCNT}})}{k_{\text{SWCNT}} + (n-1)k_{H_2O} - \phi_{\text{SWCNT}}(k_{H_2O} - k_{\text{SWCNT}})}\right]$.

The proposed conductivity model describes the shape effect of the nanoparticles that are considered for the various values of the constraint *n* used.

The similarity variable is introduced as follows:

$$u = \alpha x f'(\eta),\ \ v = -\left(\alpha\nu_f\right)^{1/2} f(\eta), \eta = y\left(\alpha/\nu_f\right)^{1/2},\ \ \theta(\eta) = \frac{T-T_\infty}{T_w(x)-T_\infty}, \tag{5}$$

so that $v_w = -\left(\alpha\nu_f\right)^{1/2} S$, where S is the constant mass flux velocity, $S>0$ designates for suction, and $S<0$ designates for injection, while $T_w = \dfrac{q_w}{k_f}\sqrt{\nu_f/\alpha} + T_\infty$. Now, we substitute (5) into Eqs (2) and (3) with boundary conditions (4) to obtain the following:

$$\frac{\chi_1}{\chi_2} f''' + ff'' - f'^2 - \frac{\chi_3}{\chi_2} Mf' - \frac{\chi_1}{\chi_2} Daf' = 0, \tag{6}$$

$$\frac{1}{\Pr}\frac{\chi_4}{\chi_5}\theta'' + f\theta' - 2f'\theta + \frac{Q}{\chi_5}\theta + \frac{Ec}{\chi_5}\left(\chi_1 f''^2 + \chi_3 M f'^2 + \chi_1 Da f'^2\right) = 0, \tag{7}$$

where $\chi_1 = \frac{\mu_{hnf}}{\mu_f}, \chi_2 = \frac{\rho_{hnf}}{\rho_f}, \chi_3 = \frac{\sigma_{hnf}}{\sigma_f}, \chi_4 = \frac{k_{hnf}}{k_f}, \chi_5 = \frac{(\rho c_p)_{hnf}}{(\rho c_p)_f}$

with renovated boundary constraints:

$$\begin{aligned} f(0) = S, \quad f'(0) = \lambda, \quad \theta'(0) = -(1/\chi_4), \\ f'(\eta) \to 0, \quad \theta(\eta) \to 0 \quad \text{as} \quad \eta \to \infty. \end{aligned} \tag{8}$$

where the primes denote differentiation with respect to η and λ is the stretching/shrinking parameter. The following are additional definitions of the terms listed above:

- M is the magnetic parameter, $M = B_0^{\,2}\frac{\sigma_f}{\alpha\rho_f}$.
- Ec is the Eckert number, $Ec = \frac{u_w^{\,2}(x)}{(C_p)_f\left(T_w - T_\infty\right)}$.
- Q is the heat source/sink parameter, $Q = \frac{Q_0}{\alpha\left(\rho C_p\right)_f}$, where $Q_0 > 0$ and $Q_0 < 0$ represent the heat source and the heat sink, respectively.
- Porous parameter, $Da = \frac{\upsilon_f}{\alpha K^*}$.

Next, we specify the following:

$$C_f = \frac{\mu_{hnf}}{\rho_f u_w^{\,2}}\left(\partial_y u\right)_{y=0}, \quad Nu_x = \frac{xk_{hnf}}{k_f\left(T_w(x) - T_\infty\right)}\left(-\partial_y T\right)_{y=0}. \tag{9}$$

Using (5) and (9), we obtain the following:

$$\mathrm{Re}_x^{0.5} C_f = \chi_1 f''(0), \mathrm{Re}_x^{-0.5} Nu_x = 1/\theta(0). \tag{10}$$

$\mathrm{Re}_x = u_w(x)x/\nu_f$ represents the local Reynolds number.

3. Methodology

A numerical solution for the proposed model is obtained. The differential equations are discretized and differentiated, leading to higher-order ones because there are insufficient initial conditions. These missing values are found by target shooting in controlled circumstances. The iterative process is carried out until a precision value of 10^{-5} is obtained. To perform the calculations, MATLAB is used with the proprietary code bvp5c. Furthermore, a log of the central processing unit (CPU) time is kept, with each computation taking 0.1346 seconds. As a result, the modified first-order ordinary differential equations (ODEs) are generated as follows:

$$f = y_1,$$

$$f' = y_2,$$

$$f'' = y_3,$$

$$f''' = \left[-y_1 y_3 + {y_2}^2 + \frac{\chi_3}{\chi_2} My_2 + \frac{\chi_1}{\chi_2} Day_2 \Big/ \frac{\chi_1}{\chi_2} \right],$$

$$\theta = y_4,$$

$$\theta' = y_5,$$

$$\theta'' = \left[\left(-y_1 y_5 + 2y_2 y_4 - \frac{Q}{\chi_5} y_4 - \frac{Ec}{\chi_5} \left(\chi_1 {y_3}^2 + \chi_3 {My_2}^2 + \chi_1 {Day_2}^2 \right) \right) \Big/ \frac{\chi_4}{\chi_5} \right].$$

The boundary conditions are as follows:

$$y_a(1) - S, y_a(2) - \lambda, y_a(5) + \left(1/\chi_4\right),$$

$$y_b(2), y_b(4) \to 0.$$

The unknown choices of the initial conditions that are not available are obtained by using the shooting technique; then, the Runge-Kutta technique is employed to solve the system initial value problems (IVPs) are considered with a step size of 0.001 and the iteration process is continued until a desired accuracy of 10^{-5} is obtained.

4. Interoperation discussion of the outcomes with validation

The two-dimensional motion of CNT-water based nanofluids past a permeable stretching/shrinking surface is presented in this article. The conducting nanofluid equipped with the dissipative heat, thermal radiation, and heat source encourages the flow phenomena. In particular, the study encounters the properties of a SWCNT and a MWCNT. The thermophysical properties associated to the nanoparticles and the conventional liquid water is displayed in Table 1. The permeability of the surface suggests the impact of suction/injection due to the external pressure exerted within the domain. Additionally, the convective boundary conditions strongly affect the flow phenomena. The transformed designed model composed of several factors is handled by the implementation of the numerical technique (i.e., the shooting based Runge-Kutta fourth order). In particular, there is a good agreement with the work of an earlier investigation considering the case of a nanofluid and the absence of certain characterizing parameters presented in Table 2. Furthermore, the validation of the results (Table 3) up to a certain degree of accuracy presents the convergence properties of the proposed methodology. Moreover, the computation of various profiles is obtained for the suggested values of the fixed parameters, where the behavior of a particular constraint within their proper ranges is deployed in the corresponding figures. The following section describes the physical behavior of the characterizing constraints that affect the flow profiles.

Table 2. Comparison with previous study $\phi_2 = Ec = M = Q = 0, \lambda = 1$.

ϕ_1	$-f''(0)$	
	Previous study [6]	Present study
0.05	1.005377897	1.005372414
0.1	0.998771585	0.998772573
0.15	0.981844588	0.981842572
0.2	0.955918876	0.955942573

Table 3. Computation of rate coefficients.

M	Da	S	λ	Ec	ϕ_1	ϕ_2	Pr	$\mathrm{Re}_x^{1/2} C_f$	$\mathrm{Re}_x^{-1/2} Nu_x$
1								−0.1671	1.9628
2								−0.1998	1.9163
3								−0.2276	1.88
1	1							−0.1671	1.9628
	2							−0.2018	1.9136
	3							−0.231	1.8757
	1	0.1						−0.1618	1.3979
		0.2						−0.1671	1.9628
		0.3						−0.1727	2.5651
		0.1	0.2					−0.3413	2.3679
			0.4					−0.7101	2.8156
			0.6					−1.1046	2.9573
			0.2	0.1				−0.1671	1.9628
				0.2				−0.1671	1.9441
				0.3				−0.1671	1.9257
				0.1	0.01			−0.1671	1.9628
					0.02			−0.1858	1.9573
					0.03			−0.2073	1.9506
					0.01	0.01		−0.1671	2.0658
						0.02		−0.1868	2.0145
						0.03		−0.2093	1.9628
						0.01	6.9	−0.1671	1.7316
							7.1	−0.1671	1.8321
							7.3	−0.1671	1.9517

4.1. Velocity profiles ($f'(\eta)$)

The current study became novel when the particle concentration of the CNT nanoparticles for the water-based hybrid nanofluid was considered. The implementation of the particle concentration enhances the thermophysical properties embedded within the system. Figure 2 depicts the

exploration of volume concentration of the nanoparticles (ϕ_1, ϕ_2) on $f'(\eta)$ in the case where the flow through a permeable medium $(Da = 1)$ and through an impermeable medium $(Da = 0)$. The volume concentration shows the percentage of the ratio among the volume of the nanoparticles and the volume of the total container. Here, $\phi_1 = 0 = \phi_2$ is used to characterize the non-appearance of the SWCNT (ϕ_1) and MWCNT (ϕ_2) nanoparticles which represent the circumstance of a pure fluid and the non-zero values $(\phi_1, \phi_2 = [0 - 0.03])$, thus suggesting the effect of concentration on the fluid velocity. The proposed figure detects that for the enhanced concentration of both the particles, the flow profiles in either of the porous/non-porous media are enhanced. The fact is very clear to observe, and it is seen that the agglomeration of the heavier particles near the surface region overshoots the velocity for which the profile enhances. The picture shows that the flow through the porous matrix significantly retards the profile rather than the flow through the clear fluid medium. Figure 3 represents the significant role of the magnetization and its behavior affecting the $f'(\eta)$ of hybrid nanofluid for the adequate values of the other contributing constraints. For the statistical behavior, the variation of the magnetic parameter is restricted within the range of 0 to 3. Here, the non-magnetized effect is presented for $M = 0$ and the variation is presented for $M \neq 0$. Applied magnetic fields induce the alignment of magnetic nanoparticles within the nanofluid. It generates either secondary flows or convection patterns within the nanofluid, thus either enhancing or suppressing heat and mass transfer rates. Inclusion of the transverse magnetic authorizes the production of a resistive force, known as the Lorentz force, which has a property to resist the fluid motion. This enforces the fluid velocity to significantly retard throughout the domain for which the bounding surface thickness also became thinner and thinner. This observation is revealed for both the case where the flow is either in a clear fluid medium or through a permeable medium. However, the permeability also acts as a resistive force similar to magnetization. This resistivity opposes the profile to enhance it. Generally, magnetic fields are used to manipulate the flow behavior of magnetic nanofluid carriers in biomedical applications, thus facilitating targeted drug delivery to specific regions within the body. Figure 4 demonstrates the explanation of the suction/injection on the fluid velocity in association with the Darcy/non-Darcy medium. The range of the parameter is bounded by -0.5 to 0.5, where the negative sign indicates the case of injection and the positive sign represents the suction velocity. Furthermore, the assigned value $S = 0$ clarifies that the flow over the surface is impermeable. Suction is an external force that is exhibited due to the flow over a permeable surface. The force that is exerted due to the external air pressure is known as suction. The result reveals that for the enhanced suction there is attenuation in the velocity profile, which is marked with an asymptotic nature of the profiles. However, in the case of injection, the magnitude of the profile is significantly enhanced. Figure 5 depicts the role of the stretching ratio affecting the $f'(\eta)$ due to the variation of the porous matrix. Here, the range of the parameter is distributed with the numerical values as -0.5 to 0.5. The negative represents the circumstance of shrinking and the positive indicates the situation of stretching. The graphical presentation detects that the profile enhances with the upsurge of the stretching ratio and in scenarios of stretching/shrinking the magnitude of the profile augments. It is seen that the case of shrinking the profile augments in the negative domain and the case of stretching the variation is presented in the positive domain. In a special case, it is exciting to observe that the profile became linear for the assigned zero values of λ.

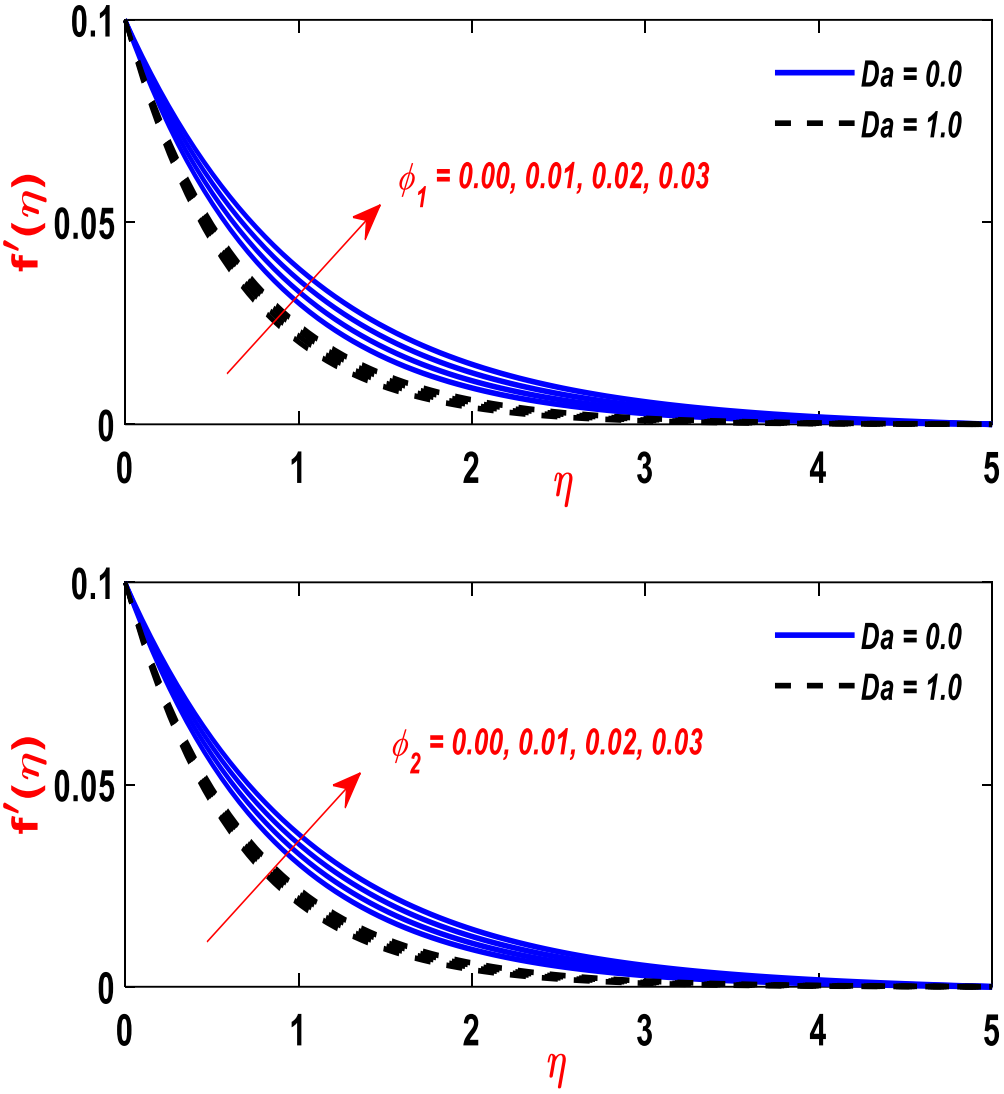

Figure 2. Graphical depiction of ϕ_1 and ϕ_2 versus $f'(\eta)$.

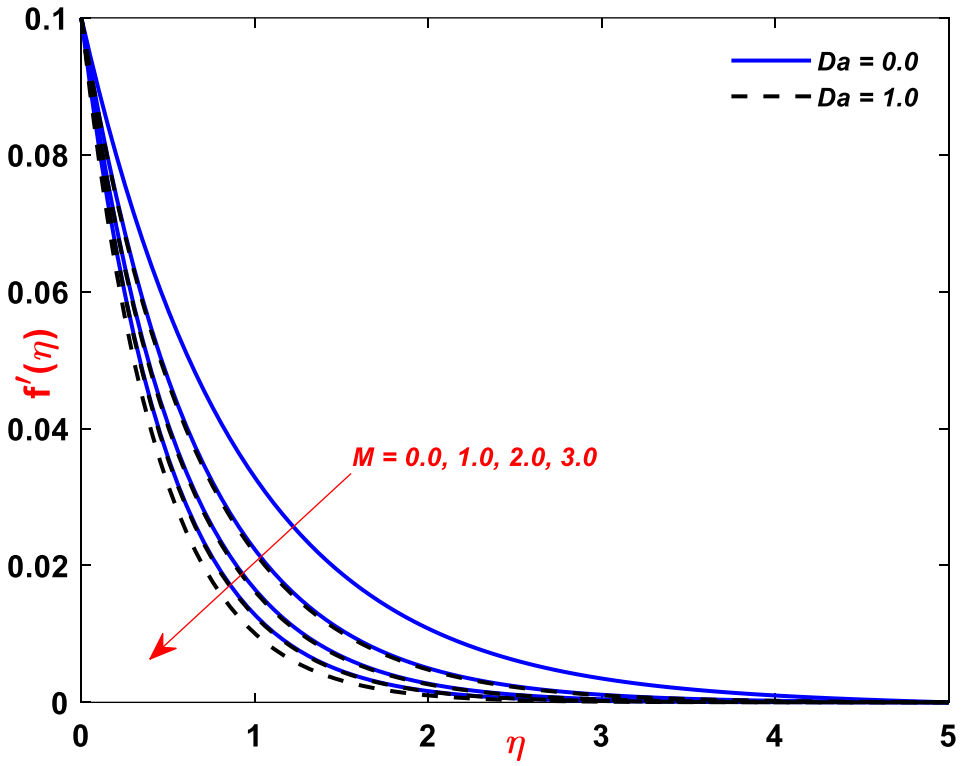

Figure 3. Graphical depiction of M versus $f'(\eta)$.

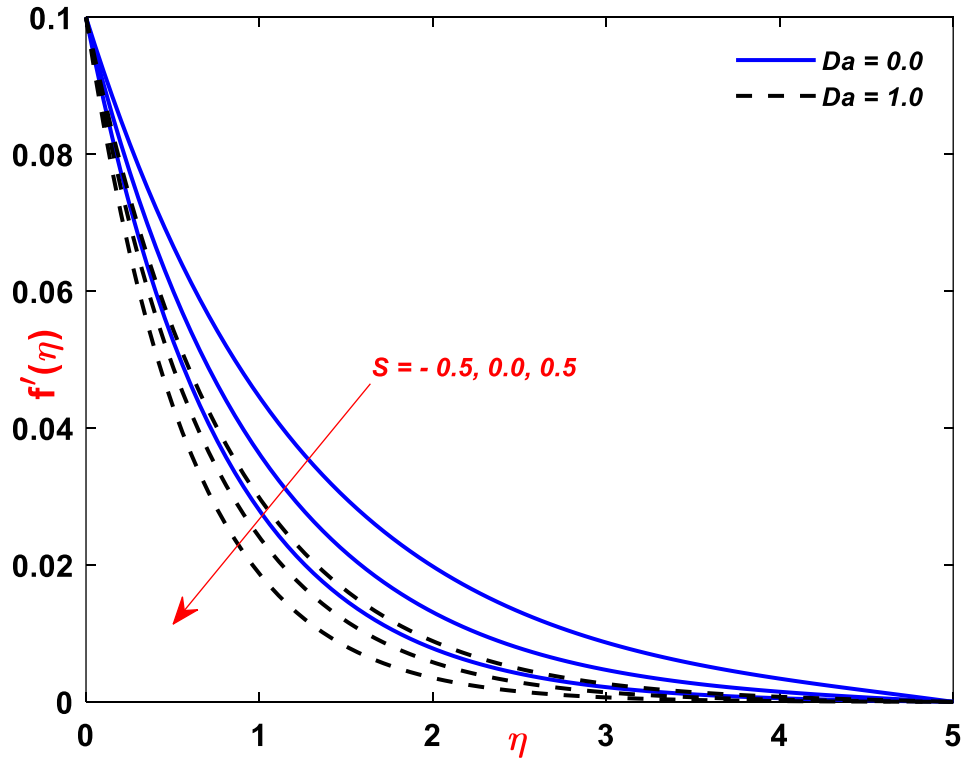

Figure 4. Graphical depiction of S versus $f'(\eta)$.

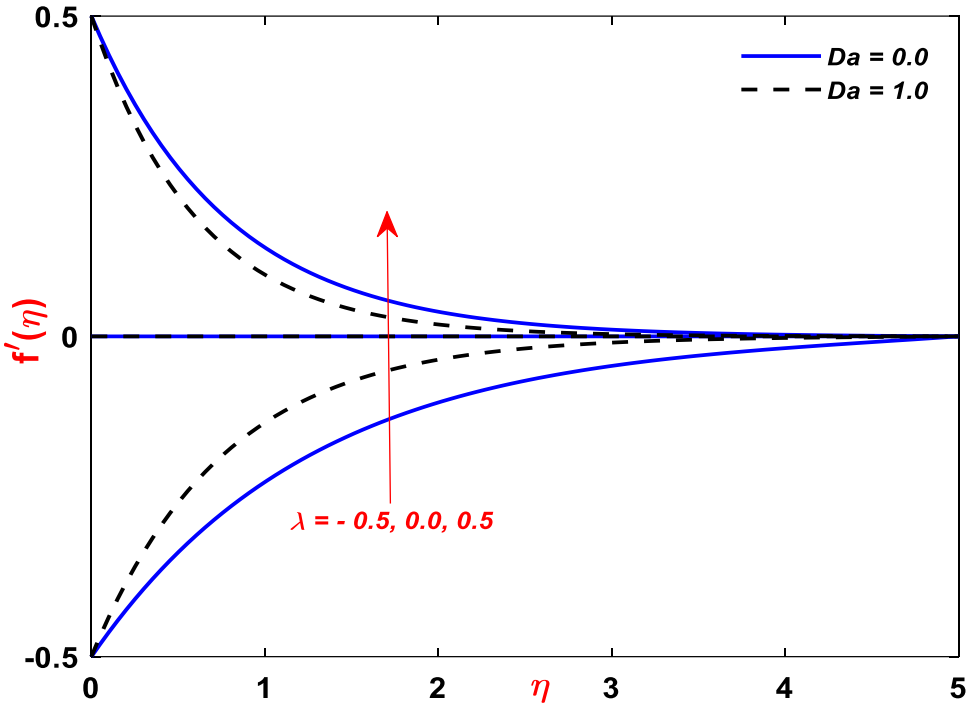

Figure 5. Graphical depiction of λ versus $f'(\eta)$.

4.2. Temperature profile $(\theta(\eta))$

One of the significant factors that enrich the flow phenomena is the nanoparticle concentration. It is useful to see that all the thermophysical properties are dependent on the construction of the particle concentration. Figure 6 depicts the characteristics of the volume concentration that affects the $\theta(\eta)$ for the variation of the porous matrix. The inclusion of the concentration of the nanoparticle enhances the thermal properties of the nanofluid due to the enhanced thermal conductivity. For the augmentation, the particle concentration overshoots the fluid temperature because the rate of agglomeration encases the energy, and the stored energy significantly overshoots the fluid temperature. Additionally, the development causes a smooth augmentation in the profile thickness with an asymptotic nature. The behavior is deployed for both the case of Darcy/non-Darcy media. The increasing porosity gradually enhances the fluid temperature in comparison to the flow through the non-Darcy medium. The resistivity of the Darcy medium resists the fluid velocity favors, which enhances the bounding surface thickness. Figure 7 explores the variation of the magnetization affecting $\theta(\eta)$ in the appearance/nonappearance of a porous matrix. The resistivity of the magnetization that resists the fluid motion favors, which significantly enhances the fluid temperature. Moreover, this enhancement is due to the flow via a porous matrix. Furthermore, the enhancing temperature profile suggests that the surface became cool. It provides a greater coolant, which is useful in various industrial applications in recent scenarios. Figure 8 portrays the favorable cases for the statistical behavior of the coupling constant, known as Eckert number, on $\theta(\eta)$. The existence of the Eckert number is because of the implementation of the dissipative heat due to the mutual effect of viscous and Joule dissipation in the energy equation. Mathematically, the construction of the Eckert

number shows an inverse relation with the temperature differences among the fluid and ambient states. As the difference retards, the value of the Eckert number increases, and the fluid temperature subsequently increases. The absence of the dissipative heat portrays a thinner thickness of the thermal bounding interface, and the higher values of the Eckert number overshoots the profile significantly. Furthermore, similar to a previous description, the result shows that increasing either the porosity or the flow via permeable medium favors augmenting the profile. Figure 9 displays the features of the supplementary heat source/sink on $\theta(\eta)$ in both of the considered media. The distributed ranges for the parameter are −0.5 to 0.5, with the special case of the absence of a heat source. The clarification reveals that the negative is used for the case of a sink and the positive is used for the impact of a heat source. The outcomes disclose that the increasing heat source significantly upsurges the fluid temperature.

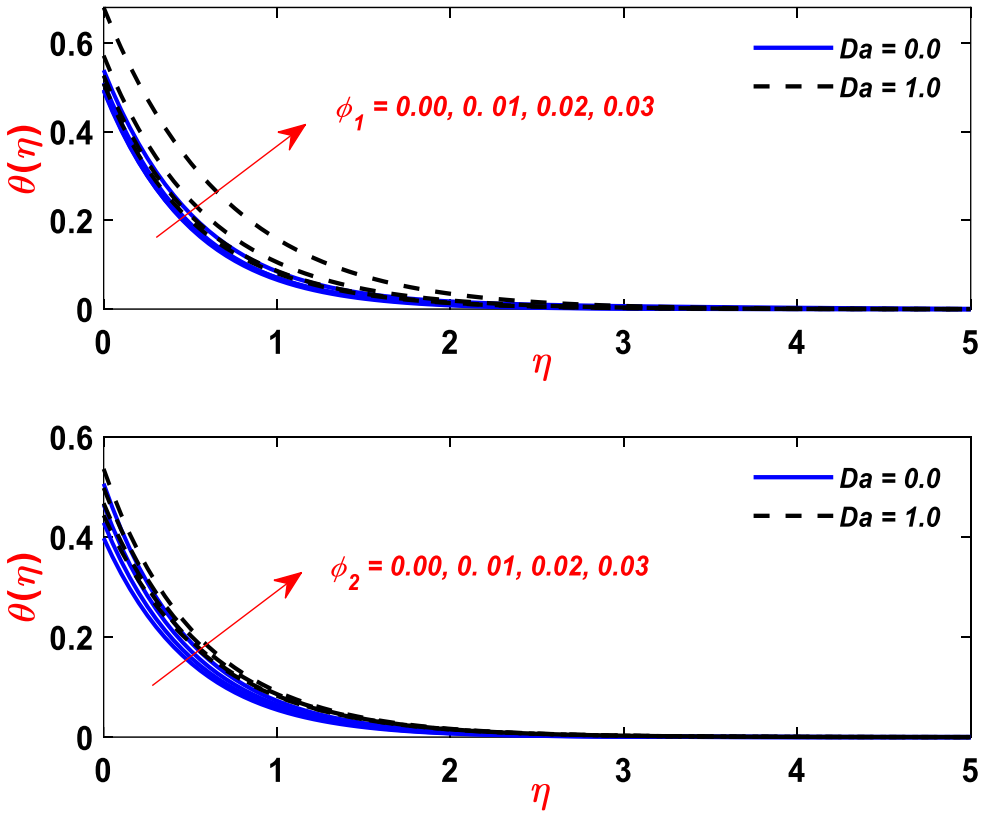

Figure 6. Graphical depiction of ϕ_1 and ϕ_2 versus $\theta(\eta)$.

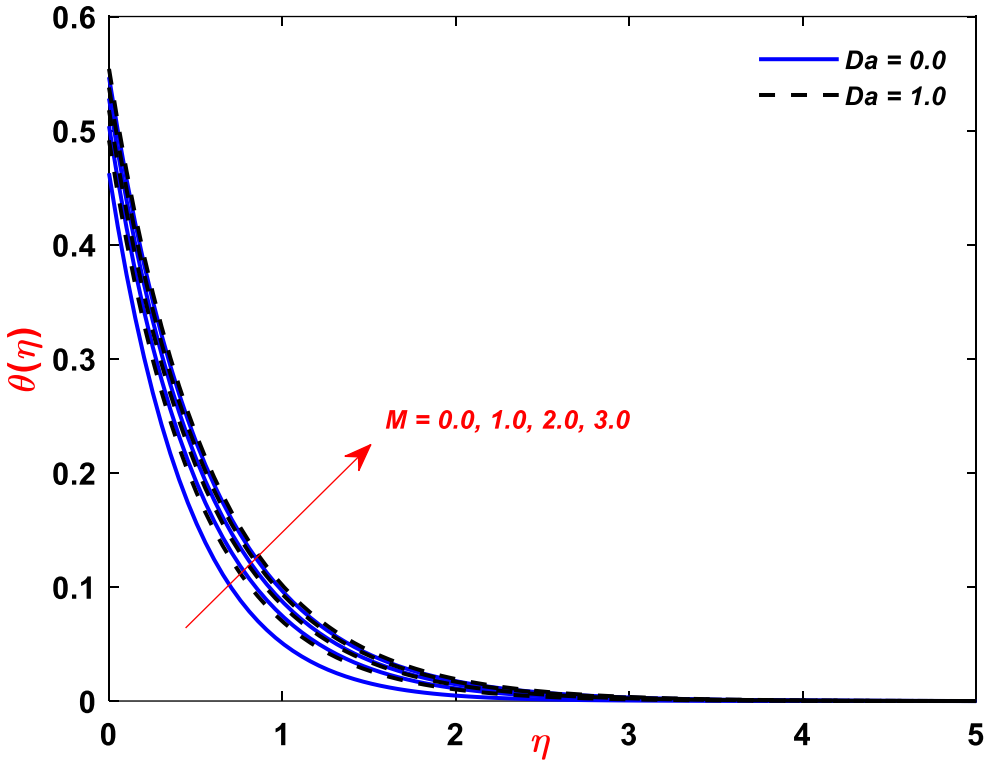

Figure 7. Graphical depiction of M versus $\theta(\eta)$.

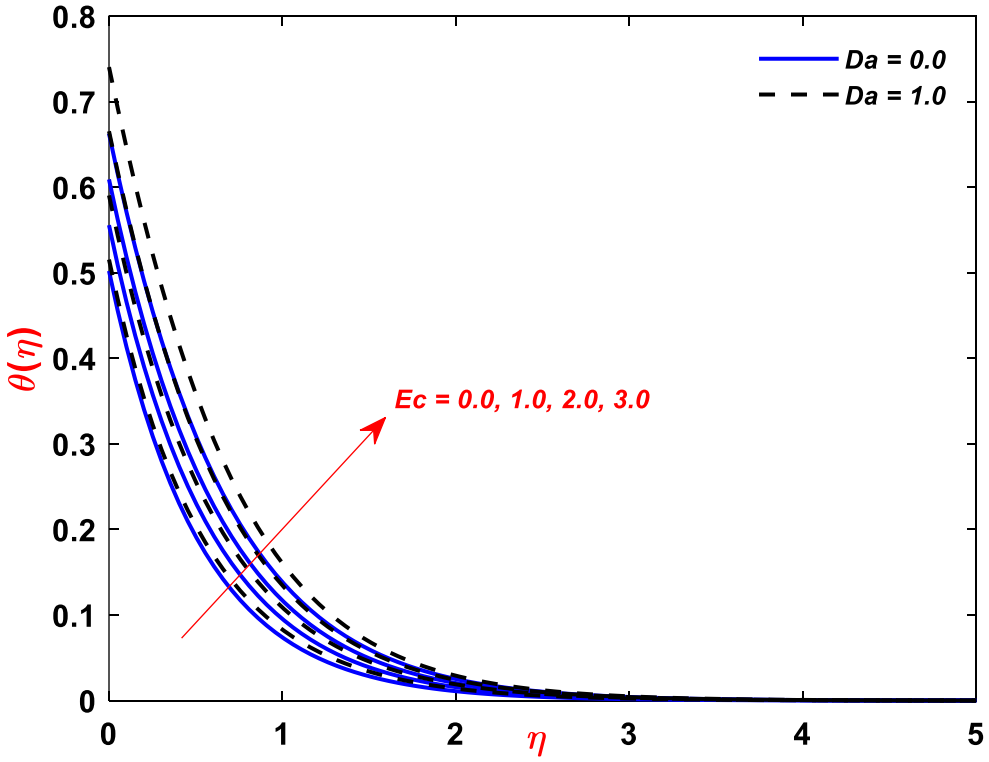

Figure 8. Graphical depiction of Ec versus $\theta(\eta)$.

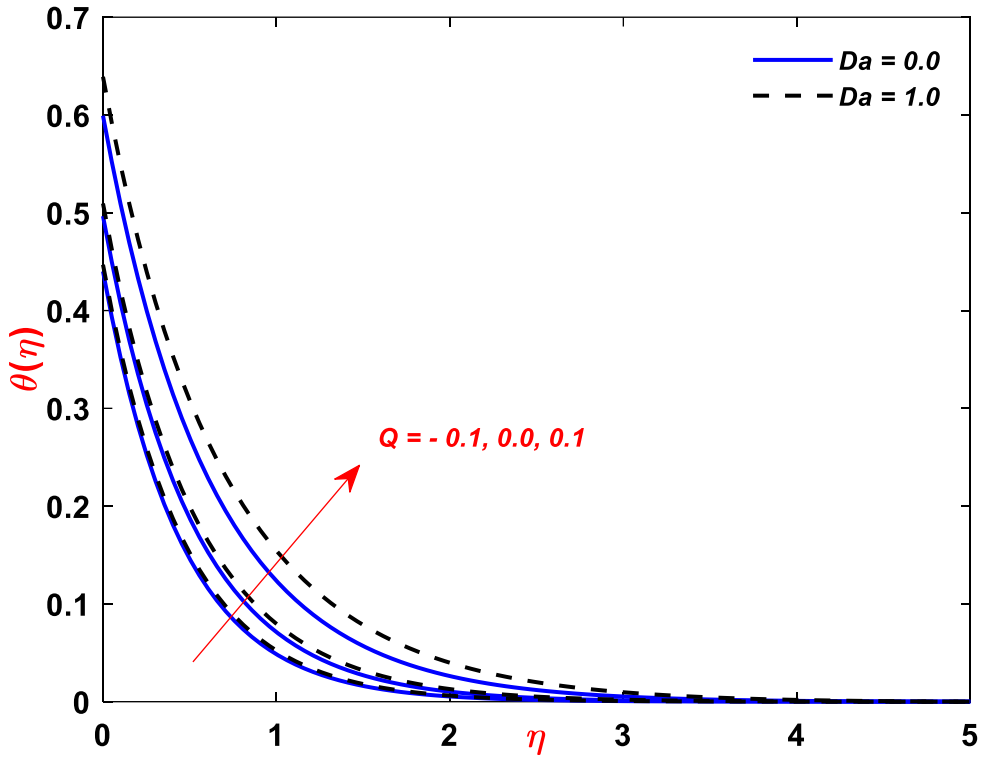

Figure 9. Graphical depiction of Q versus $\theta(\eta)$.

5. Response surface methodology (RSM)

The RSM statistical technique is used to model and analyze the relationship between a set of independent variables (factors) and a response variable (outputs). It helps in optimizing processes, improving the product quality, and sympathetic interactions between variables. The RSM involves designing experiments, fitting mathematical models to experimental data, and then analyzing these models to determine the optimal conditions to achieve the desired responses. This proves highly efficient in streamlining both modelling and experimentation processes, this resulting in time and resource savings while enhancing the overall efficiency. The central composite design (CCD) serves as a widely employed mathematical expression to generate a second-order response surface. The model for the second-order response surface is as follows:

$$\Re = \alpha_0 + \sum_{i=1}^{3} \alpha_i x_i + \sum_{i=1}^{3} \alpha_i x_i^2 + \sum_{j=1}^{3} \sum_{i=1}^{3} \alpha_i \alpha_j x_i x_j \ .$$

The suggested regression model integrates three unique effects: linear, quadratic, and interaction effects. In the CCD model, both factorial and axial runs are encompassed, with the remaining runs placed centrally. Specifically, factors such as the concentration of SWCNT and MWCNT nanoparticles, and magnetic parameters are employed to influence the heat transfer rate response. Table 4 presents a diverse range of influential factors to stimulate the heat transportation rate. This figure illustrates the distribution of 20 distinct runs (Table 5) while varying the parameter values.

Table 4. Levels of independent factors.

Parameters	Level		
	Low value (−1)	Medium value (0)	High value (+1)
$\mathbf{A}(\phi_1)$	0.01	0.015	0.02
$\mathbf{B}(\phi_2)$	0.01	0.015	0.02
$\mathbf{C}(M)$	0.1	0.2	0.15

Table 5. Design of experiment.

Runs	Actual values			Output values
	A	**B**	**C**	$\mathrm{Re}_x^{-1/2} Nu_x = Nu$
1	0.010	0.010	0.10	2.0202
2	0.020	0.010	0.10	2.0093
3	0.010	0.020	0.10	2.0697
4	0.020	0.020	0.10	2.0577
5	0.010	0.010	0.20	2.0127
6	0.020	0.010	0.20	2.0026
7	0.010	0.020	0.20	2.0626
8	0.020	0.020	0.20	2.0514
9	0.010	0.015	0.15	2.0413
10	0.020	0.015	0.15	2.0303
11	0.015	0.010	0.15	2.0113
12	0.015	0.020	0.15	2.0604
13	0.015	0.015	0.10	2.0394
14	0.015	0.015	0.20	2.0325
15	0.015	0.015	0.15	2.0359
16	0.015	0.015	0.15	2.0359
17	0.015	0.015	0.15	2.0359
18	0.015	0.015	0.15	2.0359
19	0.015	0.015	0.15	2.0359
20	0.015	0.015	0.15	2.0359

5.1. Validation of model

The ANOVA statistical method is used to partition the total variance observed in a dataset into different sources of variation. In the context of the RSM, an ANOVA helps to assess the significance of corresponding factors and their interactions on the response variable(s). It provides information on which factors have a significant effect on the response and allows for the identification of any interactions between factors. Statistical matrices, specifically the coefficient of determination (R^2), lack-of-fit tests derived using the hypothetical test followed by analysis of variance (ANOVA), are utilized to assess the model with the provided data, thus measuring its capacity to accurately capture variations in the response variables. The evaluation is carried out through Table 6 for the heat transfer rate, with standard results typically obtained at a confidence level of 95% or a 5% significance level for enhanced precision. P-values for the response corresponding to each of the three components are derived from the ANOVA results. The proposed model, which articulates the response in terms of these three factors, along with the responses of Nusselt number, are presented

through Figure 10. Additionally, the proposed coefficients for both the responses are as follows:

$$Nu = 2.03590 - 0.005520A + 0.024570B - 0.003450C - 0.000109A \times A - 0.000059B \times B + 0.000041C \times C - 0.000275A \times B + 0.000200A \times C + 0.000100B \times C.$$

The analysis indicates that the p-values gained for the Nusselt number in Table 6 for the interaction parameter below to 0.05 are treated as significant. Consequently, the proposed expression is preferable for the existing assumed values of the Nusselt number, which validates the model implying favourable outcomes. The predicted R^2 of 1.000 and the adjusted R^2 of 1.000 for Nusselt number, demonstrate a close agreement, with differences less than 0.2. The coefficient estimates in Table 7 (Nu expression) suggest a responsiveness to changes in individual factors while holding others constant.

Based upon the orthogonal design, the intercept represents the average response across all runs. Furthermore, coefficients modify this average based on the factor settings. Variance inflation factors (VIFs) help assess multicollinearity, where values greater than 1 indicate correlated factors. Generally, VIFs below 10 are acceptable, and higher values suggest stronger correlations.

Figure 11(a)–(f) display visual representations of the heat transportation rate (i.e., Nusselt number). These plots graphically depict the response function, the Nusselt number, and the proposed factors. In Figure 11(a),(b), the magnetic parameter remains constant at the central level, the contour and surface lines show an increase in the response function at higher levels. As the parameter goes from low to high values, the Nusselt number proportionately increases. Conversely, the pattern is reversed when the parameter goes from low to high values. Figure 11(c),(d) maintains a constant central value for the concentration of the WCNT, revealing a direct proportionality between the local shear rate, the increase in the concentration of the SWCNT nanoparticles, and magnetic parameter from low to high values. In Figure 11(e),(f), the observation reveals that the response function increases with enhancements in both the magnetic parameter and the concentration of the MWCNT values. However, when the values of this parameter rise from low to high, the trend falls.

Table 6. Analysis of variance (ANOVA).

Source	Degree of Freedom	Adjusted Sum of Square	Adjusted Mean of Square	F-Value	P-Value	Coefficients
Model	9	0.006462	0.000718	3159036.58	0.00000	2.03590
Linear	3	0.006461	0.002154	9475514.40	0.00000	
A	1	0.000305	0.000305	1340697.60	0.00000	−0.005520
B	1	0.006037	0.006037	26562135.60	0.00000	0.024570
C	1	0.000119	0.000119	523710.00	0.00000	−0.003450
Square	3	0.000000	0.0	121.33	0.00000	
A×A	1	0.000000	0.0	144.00	0.00000	−0.000109
B×B	1	0.000000	0.0	42.25	0.00000	−0.000059
C×C	1	0.000000	0.0	20.25	0.00100	0.000041
Interaction	3	0.000001	0.0	1474.00	0.00000	
A×B	1	0.000001	0.000001	2662.00	0.00000	−0.000275
A×C	1	0.000000	0.0	1408.00	0.00000	0.000200
B×C	1	0.000000	0.0	352.00	0.00000	0.000100
Error	10	0.000000	0.0			
Lack-of-Fit	5	0.000000	0.0			
Pure Error	5	0.000000	0.0			
Total	19	0.006462				

Table 7. Fit statistics.

Std. Dev.	0.0000	**R^2**	1.0000
Mean	2.04	**Adjusted R^2**	1.0000
C.V. %	0.0007	**Predicted R^2**	1.0000
		Adeq Precision	6292.6618

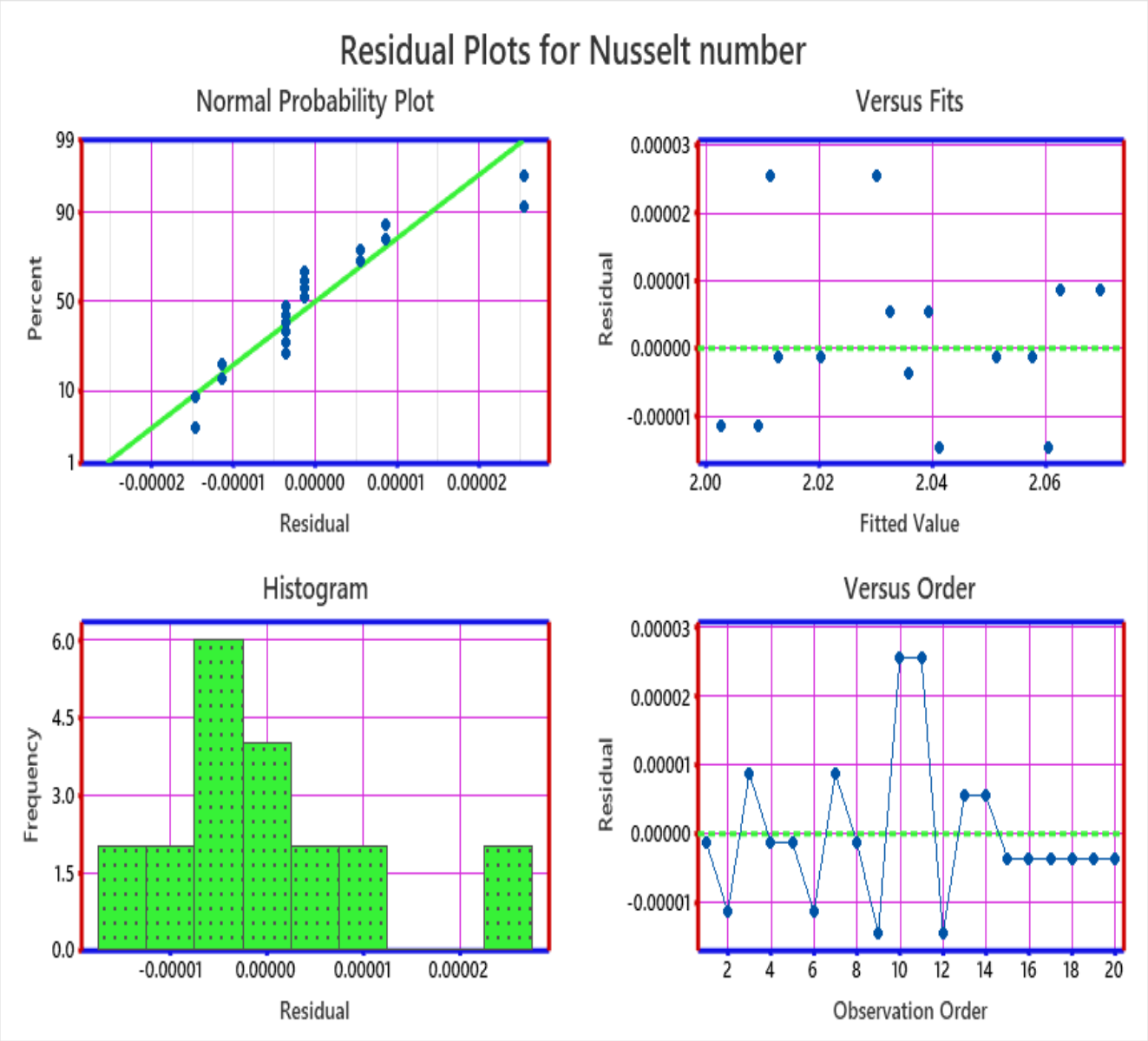

Figure 10. Residual plot.

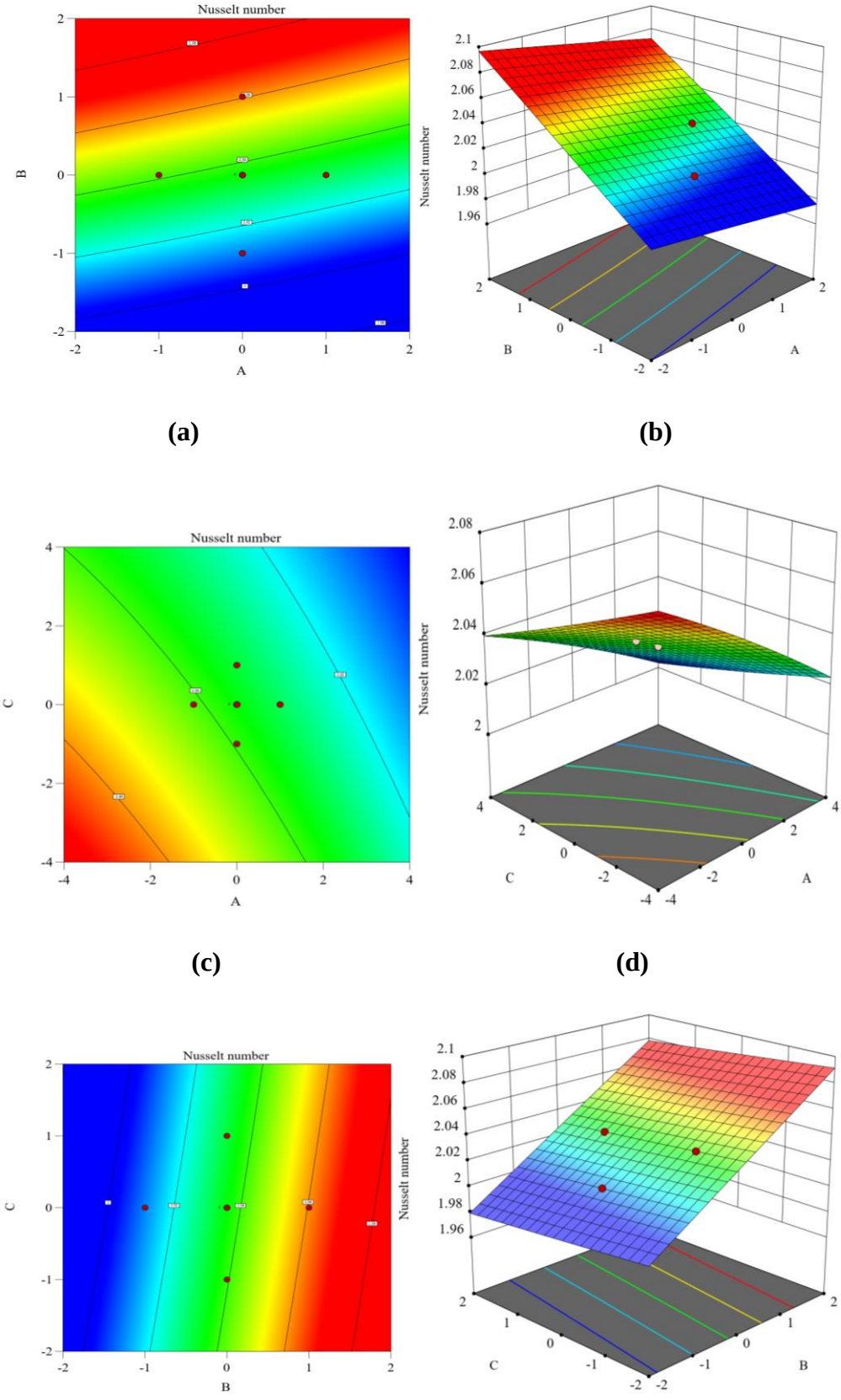

Figure 11. Contour and surface plot.

6. Sensitivity analysis

A sensitivity analysis must be incorporated into the proposed design in order for it to be effectively modelled and simulated (Table 8). This crucial stage helps designers see how the model responds to variations in the input parameters, which helps them identify important factors and make wise choices. Sensitivity analyses are a useful method to assess how different factors affect response variables. We have carefully looked into the sensitivity of the heat transfer rates under certain conditions in our current work. This investigation helps designers find parameters that are important for making decisions. An essential aspect of this analysis is the characterization of the partial derivative with respect to effective factors such as $A(\phi_1), B(\phi_2), C(\phi_3)$ as follows:

$$\frac{\partial Nu}{\partial A} = -0.005520 - 0.000218A - 0.000275B + 0.000200C$$

$$\frac{\partial Nu}{\partial B} = 0.024570 - 0.000118B - 0.000275A + 0.000100C$$

$$\frac{\partial Nu}{\partial C} = -0.003450 + 0.000082C + 0.000200A + 0.000100B\,.$$

Table 8. Sensitivity analysis of effective parameters.

B	C	Sensitivity values		
		$\frac{\partial Nu}{\partial A}$	$\frac{\partial Nu}{\partial B}$	$\frac{\partial Nu}{\partial C}$
−1	−1	−0.0054450	0.0245880	−0.0036320
	0	−0.0052450	0.0246880	−0.0035500
	1	−0.0050450	0.0247880	−0.0034680
0	−1	−0.0057200	0.0244700	−0.0035320
	0	−0.0055200	0.0245700	−0.0034500
	1	−0.0053200	0.0246700	−0.0033680
1	−1	−0.0059950	0.0243520	−0.0034320
	0	−0.0057950	0.0244520	−0.0033500
	1	−0.0055950	0.0245520	−0.0032680

The heat transfer rate's sensitivity to parameters is shown at several levels, ranging from −1, 0, 1.

Case-1: When A is set to the middle level (0) and B is set to a low level (−1), the highest and lowest sensitivities to C are −0.0034680 and −0.0036320, respectively. The highest and lowest sensitivities to B are 0.0247880 and 0.0245880, respectively. The highest and lowest sensitivities to A are −0.0050450 and −0.0054450, respectively.

Case-2: The greatest and lowest sensitivity to C are −0.0033680 and −0.0035320, respectively, when both A and B are set to middle levels (zero and one, respectively). The sensitivity values for B are 0.0246700 at the maximum and 0.0244700 at the minimum, respectively. The sensitivities to A that are highest and lowest are −0.0053200 and −0.0057200, respectively.

Case-3: With A set to a middling level (0) and B set to a high level (1), the corresponding sensitivities to C are −0.0034320 and −0.0032680, respectively. The values of 0.0243520 and 0.0245520 represent the highest and lowest sensitivities to B, respectively, and −0.0055950 is the

highest and −0.0059950 is the lowest sensitivity to A, respectively.
From the instances described above, it can be inferred that:

- The maximum sensitivity towards heat transportation is −0.0050450 for A, 0.0247880 for B, and −0.0032680 for C.
- The minimum sensitivity towards heat transportation is −0.0059950 for A, 0.0243520 for B, and −0.0036320 for C.

7. Conclusions

The proposed power law heat flux model for the water-based hybrid nanofluid comprised of CNTs over a permeable surface was briefly analyzed. The inclusion of dissipative heat in the energy equation powered the flow phenomena. Furthermore, the numerical method implemented was useful to validate the result in particular cases. As a novel approach, a robust statistical analysis was presented using an RSM to optimize the heat transportation rate while considering various factors. The validation of the result was presented utilizing an ANOVA test, and a sensitivity analysis also portrayed the optimizing heat transportation rate for these factors. Thus, the important outcomes of the study are arranged as follows:

- The validation and the conformity of the solution were obtained with an earlier investigation up to the desired accuracy, which showed a good agreement.
- Nanoparticle concentration significantly utilized both the CNTs that favored enhancing the fluid velocity as well as the heat transport phenomena.
- The retardation in the flow profiles was exhibited due to the resistive forces offered by the implementation of the magnetized property; however, it augmented the fluid temperature.
- The dissipative heat that produced the role of coupling constant (i.e., the Eckert number with the additional heat source/sink) encountered a significant hike in the fluid temperature.
- An RSM was useful to design a model which showed an optimized response for the heat transportation rate for the combined effect of the proposed factors.
- The validation of the model was exhibited due to the proposed hypothetical test organized by the ANOVA using the same factors.
- Sensitivity approach for each of the parameters was useful to obtain optimized conditions for the response of the heat transfer rate.

Finally, the proposed study was not just for a parametric analysis that was utilized in this model, but a way to present the optimized heat transfer analysis using a statistical approach with a proper validation of the result using am ANOVA test, which is a hypothetical test that provides a road map to enhance the present study with more in depth analyses using several factors that may helpful in augmenting the heat transfer rate. Utilizing these new factors, the sensitivity analysis also favors deploying new optimized models. Other than that, the proposed analysis has several engineering and industrial applications; in a recent scenario in the biomedical science, the use of a nanofluid was vital for heart pumping, artificial hearts, blood flow phenomena through arteries, drug delivery processes, etc.

Use of AI tools declaration

The authors declare they have not used Artificial Intelligence (AI) tools in the creation of this article.

Acknowledgments

This project was supported by Researchers Supporting Project number (RSP2024R411), King Saud University, Riyadh, Saudi Arabia. This work was supported by the Technology Innovation Program (20018869, Development of Waste Heat and Waste Cold Recovery Bus Air-conditioning System to Reduce Heating and Cooling Load by 10%) funded by the Ministry of Trade, Industry & Energy (MOTIE, Korea).

Conflicts of interest

The authors declare no conflict of interest.

References

1. R. Hossain, A. K. Azad, M. J. Hasan, M. M. Rahman, Radiation effect on unsteady MHD mixed convection of kerosene oil-based CNT nanofluid using finite element analysis, *Alex. Eng. J.*, **61** (2022), 8525−8543. https://doi.org/10.1016/j.aej.2022.02.005
2. U. S. Mahabaleshwar, K. N. Sneha, H. N. Huang, An effect of MHD and radiation on CNTS-Water based nanofluids due to a stretching sheet in a Newtonian fluid, *Case Stud. Therm. Eng.*, **28** (2021), 101462. https://doi.org/10.1016/J.CSITE.2021.101462
3. L. L. Lund, M. A. Fadhel, S. Dero, Z. Shah, M. Alshehri, A. Alshehri, Slip and radiative effect on magnetized CNTs/$C_2H_6O_2$+H_2O hybrid base nanofluid over exponentially shrinking surface, *J. Magn. Magn. Mater.*, **580** (2023), 170958. https://doi.org/10.1016/J.JMMM.2023.170958
4. W. N. N. Noranuar, A. Q. Mohamad, S. Shafie, I. Khan, L. Y. Jiann, M. R. Ilias, Non-coaxial rotation flow of MHD Casson nanofluid carbon nanotubes past a moving disk with porosity effect, *Ain Shams Eng. J.*, **12** (2021), 4099–4110. https://doi.org/10.1016/J.ASEJ.2021.03.011
5. M. Ramzan, S. Riasat, Z. Shah, P. Kumam, P. Thounthong, Unsteady MHD carbon nanotubes suspended nanofluid flow with thermal stratification and nonlinear thermal radiation, *Alex. Eng. J.*, **59** (2020), 1557–1566. https://doi.org/10.1016/J.AEJ.2020.04.004
6. S. R. Mishra, P. K. Pattnaik, S. Ontela, S. Panda, Characterization of shape factor with multi slip and inclined magnetized radiative Casson hybrid nanofluid transport in an expanding/contracting convective sheet, *Part. Differ. Equ. Appl. Math.*, **8** (2023), 100570. https://doi.org/10.1016/J.PADIFF.2023.100570
7. T. Elnaqeeb, N. A. Shah, I. A. Mirza, Natural convection flows of carbon nanotubesnanofluids with Prabhakar-like thermal transport, *Math. Meth. Appl. Sci.*, 2020, 1–14. https://doi.org/10.1002/mma.6584
8. A. Abderrahmane, W. Jamshed, A. M. Abed, G. F. Smaisim, K. Guedri, S. U. Devi, et al., Heat and mass transfer analysis of non-Newtonian power-law nanofluid confined within annulus enclosure using Darcy-Brinkman-Forchheimer model, *Case Stud. Therm. Eng.*, **40** (2022), 102569. https://doi.org/10.1016/J.CSITE.2022.102569
9. Y. X. Li, S. R. Mishra, P. K. Pattnaik, S. Baag, Y. M. Li, M. I. Khan, et al., Numerical treatment of time dependent magnetohydrodynamic nanofluid flow of mass and heat transport subject to chemical reaction and heat source, *Alex. Eng. J.*, **61** (2021), 2484–2491. https://doi.org/10.1016/J.AEJ.2021.07.030

10. A. M. Amer, N. I. Ghoneim, A. M. Megahed, Investigation of dissipation phenomenon of non-Newtonian nanofluid due to a horizontal stretching rough sheet through a Darcy porous medium, *Appl. Eng. Sci.*, **17** (2024), 100171. https://doi.org/10.1016/J.APPLES.2023.100171
11. Z. Ullah, A. Abbas, E. R. El-Zahar, L. F. Seddek, A. Akgul, A. M. Hassan, Significance of thermal density and viscous dissipation on heat and mass transfer of chemically reactive nanofluid flow along stretching sheet under magnetic field, *Results Eng.*, **20 (**2023), 101413. https://doi.org/10.1016/J.RINENG.2023.101413
12. R. Mahesh, U. S. Mahabaleshwar, P. N. V. Kumar, H. F. Öztop, N. Abu-Hamdeh, Impact of radiation on the MHD couple stress hybrid nanofluid flow over a porous sheet with viscous dissipation, *Results Eng.*, **17** (2023), 100905. https://doi.org/10.1016/j.rineng.2023.100905
13. P. C. Pattanaik, S. R. Mishra, S. Jena, P. K. Pattnaik, Impact of radiative and dissipative heat on the Williamson nanofluid flow within a parallel channel due to thermal buoyancy, *Proc. I. Mech. Eng. Part*, **236** (2022), 3–18. https://doi.org/10.1177/23977914221080046
14. P. K. Pattnaik, J. Pattnaik, S. R. Mishra, B. Ali, A comparative note on the free convection of micropolar nanofluid due to the interaction of buoyancy and the dissipative heat energy, *Heat Transf.*, **50** (2021), 7020–7041. https://doi.org/10.1002/HTJ.22215
15. R. Baithalu, S. R. Mishra, P. K. Pattnaik, S. Panda, Optimizing shear and couple stress analysis for the magneto-micropolar dissipative nanofluid flow toward an elongating surface: A comprehensive RSM-ANOVA investigation, *J. Therm. Anal. Calorim.*, **149** (2024), 1697–1713. https://doi.org/10.1007/S10973-023-12741-W
16. S. Panda, S. Ontela, S. R. Mishra, P. K. Pattnaik, Response surface methodology and sensitive analysis for optimizing heat transfer rate on the 3D hybrid nanofluid flow through permeable stretching surface, *J. Therm. Anal. Calorim.*, **148** (2023), 7369–7382. https://doi.org/10.1007/S10973-023-12183-4
17. S. Panda, S. Ontela, S. R. Mishra, T. Thumma, Effect of Arrhenius activation energy on two-phase nanofluid flow and heat transport inside a circular segment with convective boundary conditions: Optimization and sensitivity analysis, *Int. J. Mod. Phys. B*, 2023. https://doi.org/10.1142/S0217979224503429
18. T. Thumma, S. Panda, S. R. Mishra, S. Ontela, Mathematical modelling of heat and solutal rate with cross-diffusion effect on the flow of nanofluid past a curved surface under the impact of thermal radiation and heat source: Sensitivity analysis, *ZAMM J. Appl. Math. Mech. Z. Für Angew. Math. Und. Mech.*, **103 (**2023), e202300077. https://doi.org/10.1002/ZAMM.202300077
19. S. Panda, S. Ontela, S. R. Mishra, T. Thumma, Hybridization of artificial neural network and response surface methodology for the optimized heat transfer rate on three-dimensional micropolar nanofluid using Hamilton-Crosser conductivity model through a circular cylinder, *J. Therm. Anal. Calorim.*, **148** (2023), 9027–9046. https://doi.org/10.1007/S10973-023-12283-1
20. T. Mehmood, M. Ramzan, F. Howari, S. Kadry, Y. M. Chu, Application of response surface methodology on the nanofluid flow over a rotating disk with autocatalytic chemical reaction and entropy generation optimization, *Sci. Rep.*, **11** (2021), 1–18. https://doi.org/10.1038/s41598-021-81755-x
21. B. K. Swain, B. C. Parida, S. Kar, N. Senapati, Viscous dissipation and joule heating effect on MHD flow and heat transfer past a stretching sheet embedded in a porous medium, *Heliyon*, **6** (2020), e05338. https://doi.org/10.1016/J.HELIYON.2020.E05338
22. P. Rana, Heat transfer optimization and rheological features of Buongiorno nanofluid in a convectively heated inclined annulus with nonlinear thermal radiation, *Propuls Power Res.*, **12** (2023), 539–555. https://doi.org/10.1016/J.JPPR.2023.10.002

23. S. Hussain, A. Ali, K. Rasheed, A. A. Pasha, S. Algarni, T. Alqahtani, et al., Application of response surface methodology to optimize MHD nanofluid flow over a rotating disk with thermal radiation and joule heating, *Case Stud. Therm. Eng.*, **103** (2023), 103715. https://doi.org/10.1016/J.CSITE.2023.103715
24. P. Rana, G. Gupta, FEM solution to quadratic convective and radiative flow of Ag-MgO/H2O hybrid nanofluid over a rotating cone with Hall current: Optimization using response surface methodology, *Math. Comput. Simul.*, **201** (2022), 121–140. https://doi.org/10.1016/J.MATCOM.2022.05.012
25. P. Rana, P. K. Sharma, S. Kumar, V. Makkar, B. Mahanthesh, Multiple solutions and stability analysis in MHD non-Newtonian nanofluid slip flow with convective and passive boundary condition: Heat transfer optimization using RSM-CCD, *ZAMM J. Appl. Math. Mech. Z. Für Angew. Math. Und. Mech.*, **104 (**2024), e202200145. https://doi.org/10.1002/ZAMM.202200145
26. J. Wang, S. A. Khan, S. Yasmin, M. M. Alam, H. Liu, U. Farooq, et al., Central composite design (CCD)-Response surface methodology (RSM) for modeling and simulation of MWCNT-water nanofluid inside hexagonal cavity: Application to electronic cooling, *Case Stud. Therm. Eng.*, **50** (2023), 103488. https://doi.org/10.1016/J.CSITE.2023.103488
27. A. Raza, S. U. Khan, K. Al-Khaled , M. I. Khan, A. Ul Haq, F. Alotaibi, et al., A fractional model for the kerosene oil and water-based Casson nanofluid with inclined magnetic force, *Chem. Phys. Lett.*, **787** (2022), 139277. https://doi.org/10.1016/J.CPLETT.2021.139277
28. Y. M. Chu, K. Al-Khaled, N. Khan, M. I. Khan, S. U. Khan, M. S. Hashmi, et al., Study of Buongiorno's nanofluid model for flow due to stretching disks in presence of gyrotactic microorganisms, *Ain Shams Eng. J.*, **12** (2021), 3975–3985. https://doi.org/10.1016/J.ASEJ.2021.01.033
29. S. Farooq, M. I. Khan, A. Riahi, W. Chammam, W. A. Khan, Modeling and interpretation of peristaltic transport in single wall carbon nanotube flow with entropy optimization and Newtonian heating, *Comput. Meth. Prog. Biomed.*, **192** (2020), 105435. https://doi.org/10.1016/J.CMPB.2020.105435
30. M. I. Khan, H. Waqas, U. Farooq, S. U. Khan, Y. M. Chu, S. Kadry, Assessment of bioconvection in magnetized Sutterby nanofluid configured by a rotating disk: A numerical approach, *Int. J. Mod. Phys. B*, **35 (**2021). https://doi.org/10.1142/S021798492150202X
31. A. Hamid, R. N. Kumar, R. J. P. Gowda, R. S. V. Kumar, S. U. Khan, M. I. Khan, et al., Impact of Hall current and homogenous-heterogenous reactions on MHD flow of GO-MoS_2/water (H_2O)-ethylene glycol ($C_2H_6O_2$) hybrid nanofluid past a vertical stretching surface, *Wave. Random Complex*, 2021. https://doi.org/10.1080/17455030.2021.1985746
32. M. A. Z. Raja, M. Shoaib, R. Tabassum, M. I. Khan, R. J. P. Gowda, B. C. Prasannakumara, et al., Intelligent computing for the dynamics of entropy optimized nanofluidic system under impacts of MHD along thick surface, *Int. J. Mod. Phys. B*, **35** (2021), 2150269. https://doi.org/10.1142/S0217979221502696
33. H. Ge-JiLe, N. A. Shah, Y. M. Mahrous, P. Sharma, C. S. K. Raju, S. M. Upddhya, Radiated magnetic flow in a suspension of ferrous nanoparticles over a cone with Brownian motion and thermophoresis, *Case Stud. Therm. Eng.*, **25** (2021), 100915.
34. S. Kavya, V. Nagendramma, N. A. Ahammad, S. Ahmad, C. S. K. Raju, Magnetic-hybrid nanoparticles with stretching/shrinking cylinder in a suspension of MoS_4 and copper nanoparticles, *Int. Commun. Heat Mass*, **136** (2022), 106150. https://doi.org/10.1016/j.icheatmasstransfer.2022.106150

35. G. Rasool, W. Xinhua, L. A. Lund, U. Yashkun, A. Wakif, A. Asghar, Dual solutions of unsteady flow of copper-alumina/water based hybrid nanofluid with acute magnetic force and slip condition, *Heliyon*, **12** (2023), e22737. https://doi.org/10.1016/j.heliyon.2023.e22737
36. G. Rasool, A. Shafiq, X. Wang, A. J. Chamkha, A. Wakif, Numerical treatment of MHD Al_2O_3-Cu/engine oil-based nanofluid flow in a Darcy-Forchheimer medium: Application of radiative heat and mass transfer laws, *Int. J. Mod. Phys. B*, **38** (2024). https://doi.org/10.1142/S0217979224501297
37. G. Rasool, A. Wakif, X. Wang, A. Alshehri, A. M. Saeed, Falkner-Skan aspects of a radiating (50% ethylene glycol+ 50% water)-based hybrid nanofluid when Joule heating as well as Darcy-Forchheimer and Lorentz forces affect significantly, *Propuls. Power Res.*, **12** (2023), 428–442. https://doi.org/10.1016/j.jppr.2023.07.001
38. G. Rasool, A. Wakif, X. Wang, A. Shafiq, A. J. Chamkha, Numerical passive control of alumina nanoparticles in purely aquatic medium featuring EMHD driven non-Darcian nanofluid flow over convective Riga surface, *Alex. Eng. J.*, **68** (2023), 747–762. https://doi.org/10.1016/j.aej.2022.12.032

AIMS Press